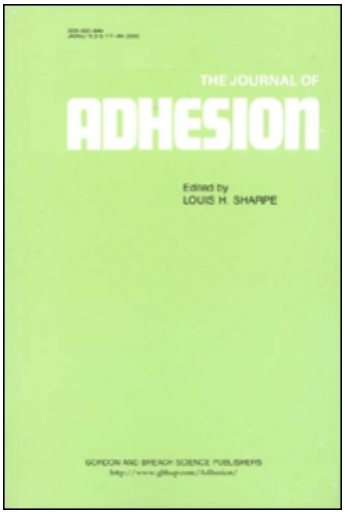

The Journal of Adhesion
Publication details, including instructions for authors and subscription information:
http://www.informaworld.com/smpp/title~content=t713453635

Interfacial Mechanical Characterization of Nicalon SiC Fiber/Alumina-Based Composites

H. F. Wu[ab]; M. K. Ferber[c]
[a] Alcoa Technical Center, Alcoa Center, Pennysylvania, USA [b] Owens-Corning, Science and Technology Center, Granville, Ohio, USA [c] Oak Ridge National Laboratory, Oak Ridge, Tennessee, USA

To cite this Article Wu, H. F. and Ferber, M. K.(1994) 'Interfacial Mechanical Characterization of Nicalon SiC Fiber/Alumina-Based Composites', The Journal of Adhesion, 45: 1, 89 — 102
To link to this Article: DOI: 10.1080/00218469408026631
URL: http://dx.doi.org/10.1080/00218469408026631

J. Adhesion, 1994, Vol. 45, pp. 89–102
Reprints available directly from the publisher
Photocopying permitted by license only

Printed in the United States of America

Interfacial Mechanical Characterization of Nicalon SiC Fiber/Alumina-Based Composites*

H. F. WU**

Alcoa Technical Center, Alcoa Center, Pennsylvania 15069, USA

and

M. K. FERBER

Oak Ridge National Laboratory, Oak Ridge, Tennessee 37831, USA

(Received October 31, 1992; in final form August 26, 1993)

Interfacial mechanical properties of both Nicalon SiC/aluminum borate and Nicalon SiC/aluminum phosphate with various fiber coatings and heat treatments were evaluated using a commercially-available indenter to induce fiber sliding during load cycling experiments. Varying degrees of sliding due to different coating materials were found. The interfacial characteristics including the shear, the residual axial fiber, and debond stresses were estimated by matching the experimental stress-displacement curves with curves predicted from an existing model. The elastic modulus and hardness of the interphase/interface in ceramic matrix composites were also evaluated. These results provided important insights into the ultimate mechanical performance of fiber-reinforced ceramic-matrix composites.

KEY WORDS Ceramic matrix composites; interfacial shear stress; nicalon fiber; aluminum borate; aluminum phosphate; nanoidentation; interphase.

INTRODUCTION

Fiber-reinforced composites are multi-phase systems in which the fiber-matrix interface is one of the most important parameters in controlling composite performance. Lamicq *et al.*[1] and Prewo and Brennan[2] have shown that high-strength ceramic fibers incorporated into brittle matrices will typically increase the fracture toughness and prevent catastrophic failure. The increase in toughness is the result of a number of energy-absorbing mechanisms that are controlled by the strength of the fiber-matrix interfacial bond as well as by the resistance to fiber sliding. Debonding, crack deflection, and fiber pull-out all contribute to improved fracture toughness and are dependent on a low bond strength at the fiber-matrix interface.[3–5] Numerous papers have been

*Presented at the International Symposium on "The Interphase" at the Sixteenth Annual Meeting of The Adhesion Society, Inc., Williamsburg, Virginia, U.S.A., February 21–26, 1993.

**Present address*: Owens-Corning, Science and Technology Center, Granville, Ohio 43023, USA.

published reporting data on the shear strength of the interface between the fiber and matrix using various test methods to obtain the data. However, there is no test method that can fully describe the fiber-matrix load transfer mechanism. To date, the single fiber pull-out test or microbond test,[6-10] the single-fiber-composite test[11-14] and the micro-indentation test[15-18] are the three most popular methods used for characterizing the interface of composite materials.

Marshall and Oliver[17] have successfully used a computer-controlled indentation system or mechanical properties microprobe (MPM)* to measure *in-situ* fiber-matrix shear stresses of frictional sliding and interface debonding in ceramic matrix composites (CMC). In their studies, the MPM, having load and displacement resolutions of 2.4 μN and 0.4 nm, respectively, was used to measure continuously the force and displacement during fiber sliding. A model describing the effects of the residual axial stress upon the stress-displacement ($\sigma - u$) curves generated during load-unload cycling was subsequently developed. The resulting expressions are summarized in Table I. In these expressions, σ is the applied stress, σ_r is the residual axial stress, R is the fiber radius, E_f is Young's modulus of the fiber in the axial direction, and τ is the interfacial shear stress accompanying fiber sliding. The parameters u_m and σ_m are the respective peak values of displacement and stress obtained during the loading cycle. For the case, $\sigma_r = 0$, the displacement upon unloading, u_o, will be equal to one-half of u_m. However, when $\sigma_r < 0\,(|\sigma| > |2\sigma_r|)$, the ratio u_u/u_m will decrease as the residual stresses becomes more compressive. When $2\sigma_r$ equals the applied stress, complete recovery occurs upon complete unloading (*i.e.*, $u_o = 0$). Finally, when the fiber is subjected to residual axial tension, u_o/u_m will exceed 0.5.

The expressions listed in Table I are based upon the assumption that a friction-bearing interface exists. If the interface is initially bonded, a finite mechanical stress (σ_d) will be required to debond the interface over a length, c. The resulting stress-displacement relationship for this case is,

$$u = (R/4\tau E_f)(\sigma)^2 (c/l)[2(1 - \sigma_r/\sigma) - (c/l)], \tag{1}$$

TABLE I
Summary of stress-displacement and stress-sliding length expressions as a function of residual axial stress in the fiber (Ref. 17)

	Total displacement	Sliding length
Loading		
$\sigma_r = 0$	$(\sigma)^2 R/4\tau E_f$	$\lvert\sigma\rvert R/2\tau$
$\sigma_r < 0\,(\lvert\sigma\rvert < \lvert 2\sigma_r\rvert)$	$(\sigma)^2 R/8\tau E_f$	$\lvert\sigma\rvert R/4\tau$
$\sigma_r < 0\,(\lvert\sigma\rvert > \lvert 2\sigma_r\rvert)$	$(R/4\tau E_f)(\sigma)^2 [1 - 2(\sigma_r/\sigma) + 2(\sigma_r/\sigma)^2]$	$[\lvert\sigma\rvert - \lvert\sigma_r\rvert]R/2\tau$
$\sigma_r > 0$	$(R/4\tau E_f)(\sigma)^2 [1 + 2\lvert\sigma_r/\sigma\rvert]$	$[\lvert\sigma\rvert + \lvert\sigma_r\rvert]R/2\tau$
Unloading		
all cases	$u_m - (\sigma_m - \sigma)^2 R/8\tau E_f$	$[\lvert\sigma_m - \sigma\rvert]R/4\tau$

*Nanoindenter Mechanical Properties Microprobe, Nano Instruments Inc., Knoxville, TN, USA.

where l is the sliding length pertaining to the unbonded interface at the same applied stress ($\sigma_r = 0$). The debond length, which can be calculated by considering the energy changes occurring during crack extension, is given as,

$$[1 - (\sigma_r/\sigma) - (c/l)]^2 = (8E_f\Gamma)/(\sigma^2 R) \quad (2)$$

where 2Γ is the fracture energy for Mode II loading at the fiber/matrix interface. The debond stress can be represented as a function of σ_r and Γ by combining Equations 1 and 2 and letting $u = 0$,

$$(R/4E_f)(\sigma_d - \sigma_r)^2 = 2\Gamma. \quad (3)$$

The expressions in Table I* provide a convenient means for evaluating the debonding, shear, and residual axial stresses from the load-displacement curves generated during cyclic loading experiments. If no debonding is required to initiate fiber sliding, then one must simply adjust the parameters σ_r and τ until the predicted and experimental curves coincide. The choice of the appropriate expression in Table I is based upon the magnitude of u_o/u_m: $\sigma_r < 0$ for $u_o/u_m < 0.5$, $\sigma_r = 0$ for $u_o/u_m = 0.5$, and $\sigma_r > 0$ for $u_o/u_m > 0.5$. If fiber debonding is observed, one must also choose a value for Γ such that the predicted loading curve, which is determined from Equations 1 and 2, exhibits the appropriate debond stress (Equation 3). The unloading curve is still predicted from the appropriate expression in Table I provided that $\sigma_m > 2\sigma/\sigma_d$.

OBJECTIVES

A primary objective of this study was to evaluate the interfacial mechanical properties of Nicalon SiC fiber/aluminum borate and Nicalon SiC fiber/aluminum phosphate composites as a function of varying fiber coatings, heat treatments, and processing using the MPM. In these newly-developed CMC systems, varying degrees of bonding due to different coating materials can control the interfacial bonding and sliding resistance or protect the fibers from environmental degradation. A secondary objective of this study was to characterize the interface/interphase in the composites by measuring elastic modulus and hardness across the fiber-matrix reaction zone. These parameters are essentially important to CMC design. In addition, understanding the effect of varying the fiber coating thickness on the relationship between the interfacial mechanical properties and CMC composite strength may provide an insight into the ultimate mechanical performance of ceramic matrix composites.

EXPERIMENTAL PROCEDURES

Specimen Preparation

Nicalon SiC fiber/aluminum borate (ALBO) composites were produced by slurry infiltration of Al_2O_3 and B_2O_3 dispersed in Nicalon fiber satin cloth using the aqueous

*By definition, the applied stresses in Table I and Eqs. 1 to 3 are negative while the displacements are positive.

and polymeric binder systems. The infiltrated cloth performs were consolidated by reaction sintering to produce an $9Al_2O_3 \cdot 2B_2O_3$ matrix. Thirteen Nicalon SiC/aluminum borate samples (designated as samples A through L) with different fiber coatings, heat treatments, and processing methods were prepared. Carbon and duplex (carbon and boron nitride) coatings were used for improving the fracture toughness of fiber-matrix interfaces. The dimension of carbon or duplex coating was about 2000 Angstrom units (0.2 μm). Two Nicalon SiC fiber/aluminum phosphate (ALPO) composites (samples N and O) were prepared by a proprietary infiltration process. Sample N was prepared using uncoated Nicalon fibers in the ALPO matrix while Sample O was fabricated with carbon-coated Nicalon fibers. Sample descriptions are listed in Table II.

Specimens examined with the MPM were prepared using conventional metallographic techniques. To prevent the lucite in the metallographic procedure from infiltrating the composites, which typically exhibited 30% porosity, the surfaces of samples were carefully covered by a thin layer of aluminum foil. The metallographic samples were then ground and polished to a 0.25 μm finish.

MPM Operation

The MPM is a special microhardness tester capable of operating at loads in the microgram range. As shown in Figure 1, the instrument consists of three major components: (1) the indenter, (2) an optical microscope, and (3) a precision table that transports the specimen between the microscope and the indenter. The indenter employs a Berkovich pyramidal diamond indenter having the same depth-area ratio as a Vickers diamond tip indenter. The angle between any of the indenter facets and its base is 60.3°. Unlike conventional hardness testers, it is not necessary to determine optically the area of an indent in order to calculate hardness. Instead, the position of the

TABLE II
Description of specimens of the ceramic matrix composites

Specimen	Id No.	Description	Condition
A	650386	Uncoated Nicalon/ALBO with polymeric binders	As-produced
B	650386	same as above	heat treated in air 1 hr @ 816°C
C	650387	Duplex-coated Nicalon/ALBO with polymeric binder	As-produced
D	650387	same as above	heat treated in air 1 hr @ 816°C
E	650388	Carbon-coated Nicalon/ALBO with polymeric binders	As-produced
F	650388	same as above	heat treated in air 1 hr @ 1200°C
H	579541	Specimen produced via S#650386,then CVD coated with SiC	heat treated in air 1 hr @ 816°C
I	650501–1	Uncoated Nicalon/ALBO with aqueous binders	heat treated in air 1 hr @ 816°C
J	650034–1	Duplex-coated Nicalon/ALBO with aqueous binders	As-produced
K	650034–1	same as above	heat treated in air 1 hr @ 816°C
L	650389	Uncoated Nicalon/ALBO with polymeric binders sintered in N_2 atmosphere	As-produced
N	639635	Uncoated Nicalon/ALPO	As-produced
O	639640	Carbon-coated Nicalon/ALPO	As-produced

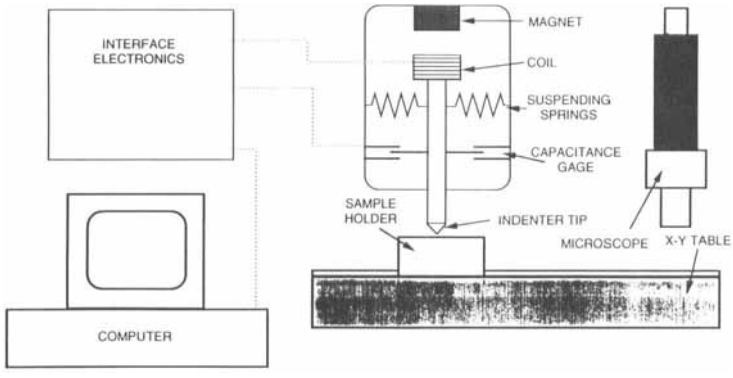

FIGURE 1 Schematic diagram of the mechanical properties microprobe.

indenter relative to the surface of the specimen is constantly monitored, thus allowing the depth of an indent to be determined. The area of the indent is then calculated from a knowledge of the geometry of the tip of the diamond indenter. The fact that the precision of the indenter can be determined to ± 0.2 nm means that the indenter can be used to sample very small volumes of material. Typical applications include the characterization of thin films, near surface properties, and the different phases in a multiphase material. A detailed description of the MPM system is given in Reference 19.

During an indentation, the load and displacement are measured continuously so that hardness can be determined as a function of indent depth on the basis of a single indent. The elastic modulus of a material also can be determined from the measurement of the slope of the unloading curve. As discussed in Section 1, the instrument is also useful in studies of composite materials and in the determination of the sliding interfacial shear stress, the residual axial stress, and the debond stress in such materials.

Test Procedures

In the case of the fiber sliding studies (designated as Phase I), the MPM was used to generate load (or stress) *versus* total displacement (u_t) curves for a minimum of ten fibers for each composite. The cyclic loading procedure adopted for this investigation is summarized in the loading history diagram in Figure 2. The fiber loading history involved an application of a predetermined constant loading rate to a maximum force, followed by a constant unloading rate until 95% of the force was removed. This sequence was followed first by a hold segment, necessary for correction of thermal drift, and then by complete unloading. The magnitudes of the force and displacement were continuously measured during each segment of the indentation procedure. The maximum load for each load/unload cycle was 120 mN.

In order to generate fiber displacement, u_s, *versus* stress, σ, curves from the MPM data, the indenter penetration into the fiber (u_p in Figure 2) was first subtracted from the total displacement of the indenter ($u_p + u_s$). This subtraction process is illustrated in Figure 3. The solid line represents the raw data generated by the MPM. The relationship between stress and u_p (dashed line in Figure 3) was previously determined by

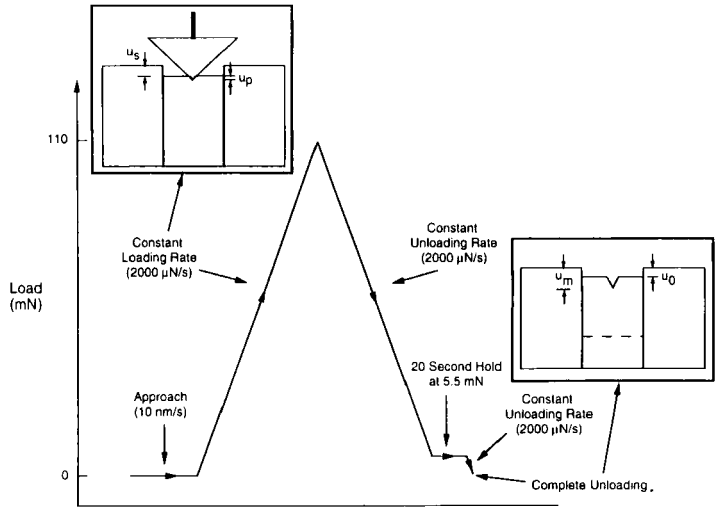

FIGURE 2 Indenter load/unload procedure used for Phase I measurements.

applying the loading procedure to several SiC fibers which did not slide. In order to facilitate the subtraction of the u_p from the total displacement *versus* stress curves, the stress dependence of u_p was represented by two curve-fitted polynomial expressions each describing the loading and unloading curves, respectively.

Microscopic observations were used to verify the existence of sliding for each fiber loaded with the MPM. Typical optical micrographs of Nicalon SiC fiber in ALPO and ALBO ceramic matrices after indentation are shown in Figure 4.

In the phase II study, we arbitrarily selected an uncoated Nicalon fiber for the evaluation of elastic modulus and hardness of the interfacial region. These properties

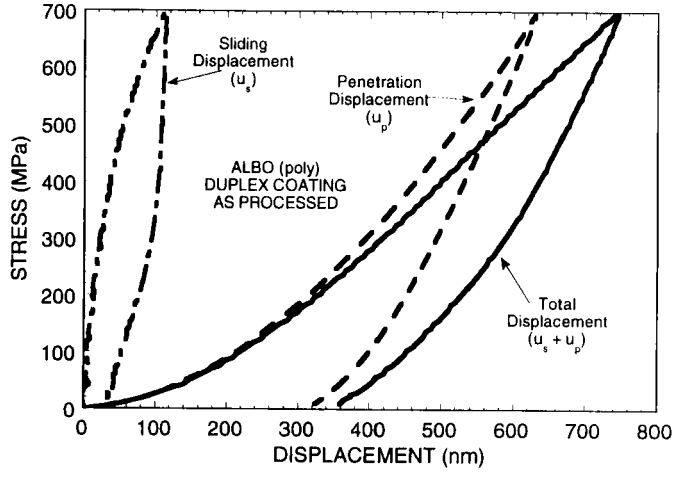

FIGURE 3 Schematic representation of the subtraction of the indenter penetration into the fiber end from the total displacement.

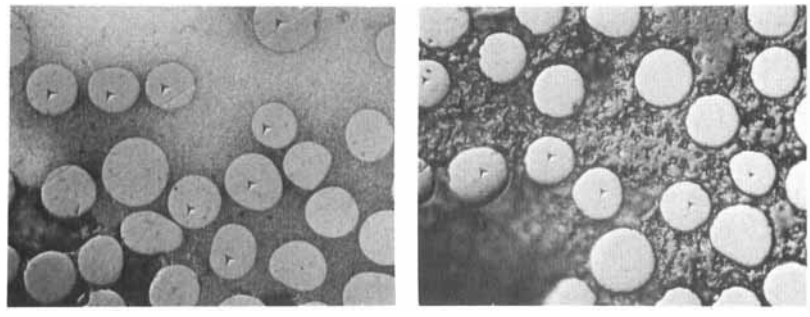

FIGURE 4 Optical micrographs of uncoated Nicalon SiC fibers in, a) ALPO and b) ALBO matrices after nanoindentation: X1000.

were measured by generating a 32-indent array which covered the bulk matrix of aluminum phosphate, the interphase zone, and the fiber cross-section. The array geometry is shown in Figure 5. Each indent was generated by loading to a force sufficient to cause a 50 nm penetration into the specimen and then unloading. The maximum depth of 50 nm was used to reduce interactions between adjacent indents.

RESULTS AND DISCUSSION

Phase I Study

Table III provides a summary of the estimates of the sliding interfacial shear stress determined by matching the experimental stress-displacement curves with the model

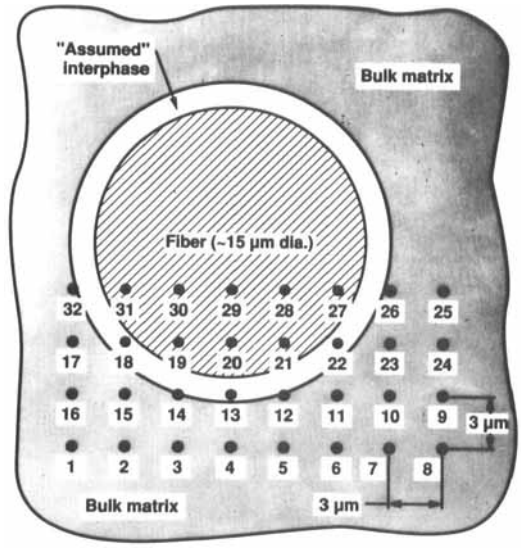

FIGURE 5 Schematic representation of thirty-two indent shapes on an uncoated Nicalon/ALPO composites.

TABLE III
Results of fiber-matrix interfacial shear stress (τ) in Nicalon SiC/ALBO and SiC/ALPO composites

Specimen	Id No.	No. of Fibers Indented	Matrix[a]	Conditions[b]	Coating	τ(MPa)	Standard Deviation (MPa)
A	650386	6	ALBO Poly	AP	None	17.2	8.64
B	650386	14	ALBO Poly	HT 816°C	None	7.38	1.98
H	650386	10	ALBO Poly	HT 816°C	CVD SiC	(c)	
C	650387	8	ALBO Poly	AP	Duplex	15.2	5.13
D	650387	10	ALBO Poly	HT 816°C	Duplex	(c)	
E	650388	5	ALBO Poly	AP	Carbon	2.94	1.99
F	650388	10	ALBO Poly	HT 1200°C	Carbon	(c)	
I	650501-1	10	ALBO Aq	HT 816°C	None	(c)	
J	650034-1	9	ALBO Aq	AP	Duplex	12.01	5.14
K	650034-1	9	ALBO Aq	HT 816°C	Duplex	1.75	1.21
L	650389	6	ALBO Poly	AP N_2	None	34.11	6.13
N	639635	9	ALPO	AP	None	(c)	
O	639640	4	ALPO	AP	Carbon	40.2	11.6

(a) Matrix processed with either polymeric binders (Poly) or aqueous binders (Aq).
(b) AP = As processed and HT = Heat Treated.
(c) Fiber sliding in these composite systems was too small to be measured.

predictions. The choice of the model parameters, τ, σ_r, and Γ, were determined by first letting $\sigma_r = \Gamma = 0$ and varying τ until the experimental and predicted values of u_m were comparable. Next, the value of σ_r was adjusted so that the predicted normalized residual displacement, u_o/u_m, matched that of the experimental data. This iterative process of varying τ and then σ_r was repeated until an acceptable match between the experimental and predicted curves was obtained. For those composites in which debonding preceded fiber sliding ($|\sigma_d| > 0$), Equations 1 and 2 were used to generate the loading curves. In this case, the debond fracture energy, 2Γ, was calculated from Equation 3 using values of σ_d measured directly from the experimental sliding curve and σ_r, estimated above. In all fits, σ_d and σ_r were constrained by the condition $|\sigma_d| \geq |2\sigma_r|$ since for $|\sigma_d| < |2\sigma_r|$, spontaneous debonding occurs prior to the application of any external load.

For those composites in which sliding could be measured, the predicted stress-displacement curves generally provided a good description of the experimental data. Figures 6a through c provide comparisons between predicted and experimental trends for several of the composite systems listed in Table III. Note that, in all cases, sliding began at the onset of loading indicating that the debond stress was negligible for these composites. However, for composites specimens H, D, F, I, and N, sliding could not be measured. This could be attributed to either a very high value of τ or a high degree of chemical bonding such that the debond stress exceeded the maximum applied stress.

As indicated in Table III, the as-processed ALBO composites fabricated using polymeric binders exhibited relatively low values of τ(< 20 MPa). The application of the duplex coating had no significant effect upon the sliding resistance. However, when carbon was used as the coating, τ was reduced to 2.9 MPa. As discussed below, these variations could be attributed to the influence of coatings upon the coefficient of friction, μ. With the exception of Specimen B, the primary effect of the heat treatment

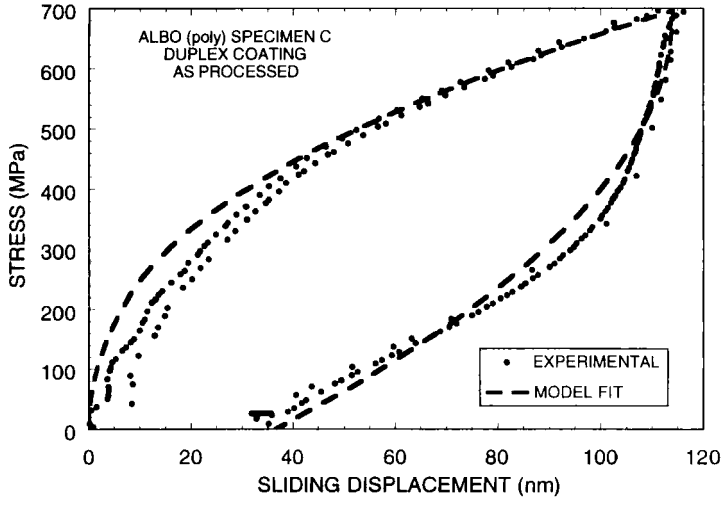

FIGURE 6a–c Typical examples of stress-displacement curves.

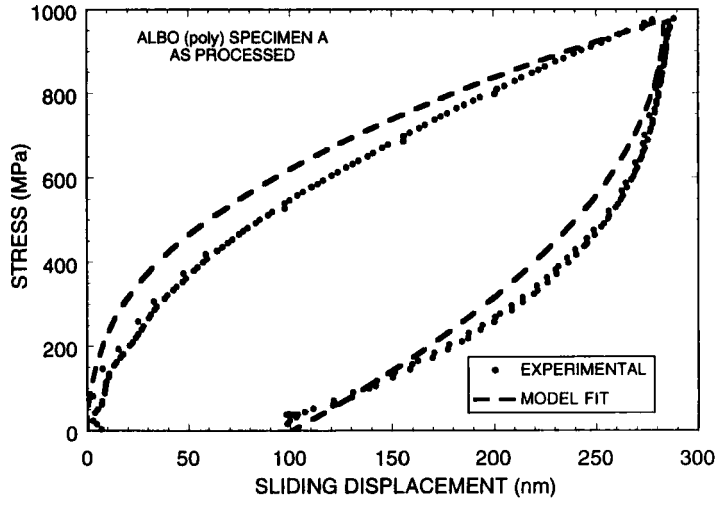

FIGURE 6(b)

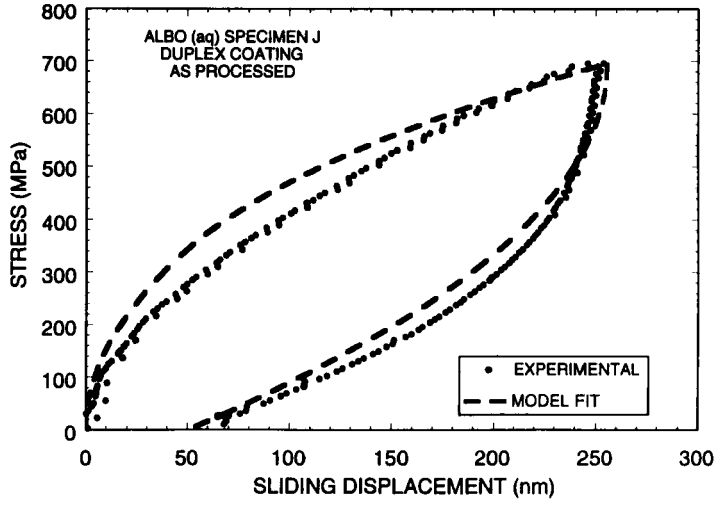

FIGURES 6(c) Typical examples of stress-displacement curves.

was to decrease the magnitude of sliding below the measurement capability of the MPM. Finally, when the ALPO composite processed with polymeric binders was densified in nitrogen (Specimen L), τ was significantly larger.

In the case of the ALPO and ALBO (aqueous binders) composites, sliding in the as-processed specimens (I and N) was below the measurement capability of the machine. The utilization of carbon and duplex fiber coatings was effective in lowering the τ values. A further lowering of the interfacial sliding shear stress was obtained for

the ALBO composite processed with aqueous binders and a duplex fiber coating by the application of 816°C heat treatment (Specimen K).

In the Marshall-Oliver model, τ is given simply by the product of the coefficient of friction, μ, and the residual clamping stress, σ_c, which is determined by (1) the differences in the thermal expansion coefficients between the matrix and the fiber and (2) the fiber roughness. Therefore, the differences in τ, reported on Table III, can be attributed to variations in one or both of these parameters. In the case of the heat-treated ALBO composites fabricated using polymeric and aqueous binders with uncoated fibers (Specimens B and I, respectively), the lower value of τ for the polymeric-based composite was probably a due to a lower value of μ. Because these composites were composed of identical matrix and fiber materials, one would not expect significant differences in the respective thermal expansion coefficients and, thus, the magnitudes of σ_c. However, the application of fiber coatings may have influenced both μ and σ_c.

Assuming that the surface roughness did not contribute significantly to the generation of radial clamping stresses during sliding, the residual axial stress in the fiber could be used to calculate σ_c from the appropriate thermal-elastic model. For all of the composites exhibiting measurable sliding in this study, the estimated values of σ_r were in the range of -50 to -100 MPa. However, these values were subject to considerable uncertainty particularly when τ exceeded 15 MPa. This uncertainty was due in the experimental error associated with the measurement of the unloading curve and, thus, the residual displacement at complete unloading. Note that in the Marshall-Oliver model, σ_r is uniquely determined by the ratio of the residual displacement to the displacement at peak stress. Consequently, the separation of the effects of μ and σ_c based upon the estimates of σ_r will require additional measurements.

Phase II Study

The purpose of this study was to investigate the hardness and modulus of the fiber-matrix interphase. In this study, an uncoated Nicalon SiC fiber/ALPO composite was selected. One particular fiber was chosen, and an array consisting of 32 indents was made to cover the bulk matrix, the interphase, and the fiber cross-section. The distance between indents was 3 μm in both the X and Y directions. The nominal total indentation displacement was 50 nm for all indents. This indentation array geometry is shown in Figure 5.

For each indent, the slope of the unloading curve at peak load was used to determine the stiffness. Using the methodology of Doerner and Nix[19] this stiffness value was used to estimate the elastic modulus and the plastic depth. The hardness was then calculated by dividing the peak load by the plastic area which was determined from the plastic depth and the geometric factor associated with the shape of the diamond indenter.

The values of the hardness and modulus for these 32 indents are listed in Table IV. The bar graph plots of hardness and modulus are shown in Figures 7a and b. These graphs reveal the difference in both modulus and hardness values between the fiber and the matrix. The average values for the moduli and hardness of the fiber and the matrix were calculated. The average modulus of the Nicalon fiber was 249 ± 12 GPa as compared with 172 ± 16 GPa for the matrix, while the literature reported that the tensile moduli of the Nicalon fiber and the alumina were about 200 GPa and 250–400 GPa, respectively.

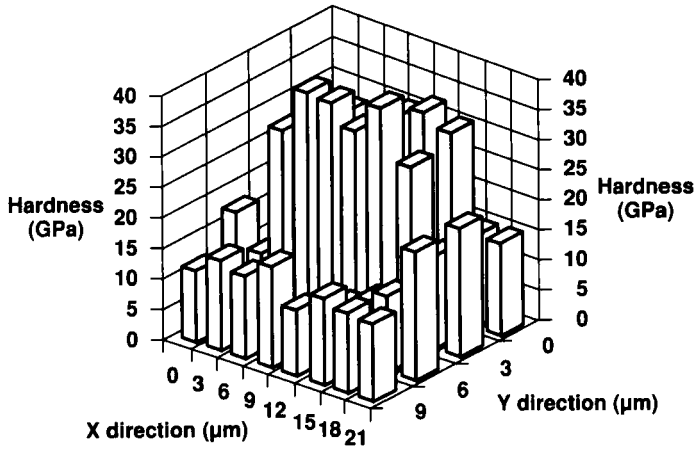

FIGURE 7a Hardness as revealed in a sequence of traverses across a transverse section of a Nicalon Fiber in ALPO matrix (the nominal total indenter displacement was 50 nm).

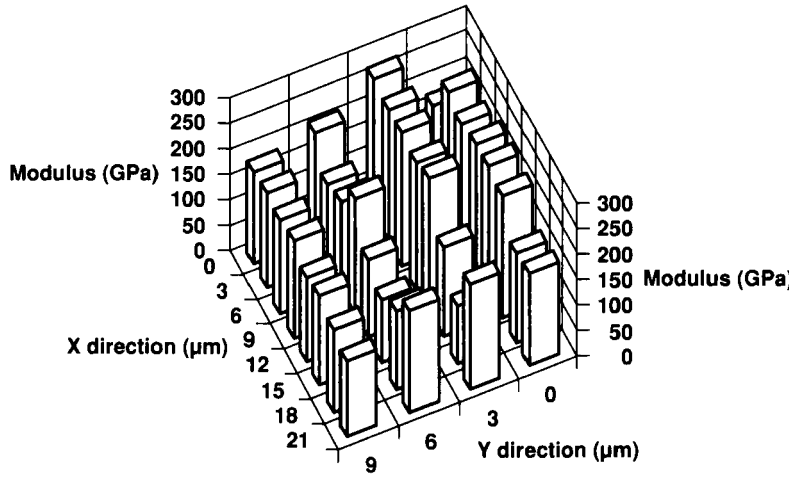

FIGURE 7b Modulus calculated from a series of indent traverses across a Nicalon fiber in the ALPO matrix (the nominal total indenter displacement was 50 nm).

Corresponding hardness values were 31.1 ± 3.3 and 13.3 ± 1.7 GPa. In addition, note that the modulus obtained from the MPM was the compressive modulus, not tensile modulus. The smaller value of the modulus of the matrix may possibly be caused by the 30% porosity of the CMC samples. The uncertainties stipulated are the standard deviations from the averages. The results from the first eight indents (the traverse in the X direction with $Y = 9\,\mu m$) were used for calculating modulus and hardness for the matrix. For the fiber, the data were obtained from 10 indents in the third and fourth traverses, the indents being selected on the basis that they seemed clearly to be on the fiber. The values obtained here are somewhat relative, not absolute values.

TABLE IV
Results of hardness and modulus of thirty-two indents at 50 nm nominal total indenter displacement (Indentation array as shown in Figure 5)

Indent #	Hardness (GPa)	Modulus (GPa)	Indent #	Hardness (GPa)	Modulus (GPa)
1	11.63	173.2	17	26.72	267.4
2	14.41	186.2	18	34.63	257.4
3	13.47	182.3	19	34.83	259.5
4	16.43	191.4	20	32.26	246.6
5	10.76	161.3	21	36.85	264.4
6	13.95	175.3	22	28.25	180.1
7	12.85	158.9	23	15.21	115.9
8	12.95	144.9	24	21.07	204.5
9	20.43	201.7	25	14.98	178.6
10	11.95	152.5	26	14.86	175
11	9.82	127.8	27	30.28	236.9
12	7.84	149.8	28	32.12	244.5
13	31.78	223.4	29	30.5	239.9
14	22.56	172.7	30	27.75	231.6
15	11.39	155.3	31	27.89	245.5
16	17.57	210.9	32	14.81	175.8

The area which we are interested in is the fiber-matrix interphase (*i.e.*, the matrix in the immediate vicinity of the fiber). The results suggest the possibility that the matrix has different properties in the immediate vicinity of the fiber but we would have to say that we really do not have enough data to be sure. Thus, some additioinal work should be carried out to answer this question.

Using the indentation test to characterize the fiber-matrix interfacial mechanical properties can help material scientists to understand how to control fiber-matrix interface in composites and can help designers by providing important insight into the ultimate mechanical performance of fiber-reinforced ceramic matrix composites.

CONCLUSIONS

Based on the findings from this study, several conclusions may be drawn as follows:

1. The MPM can be used for the determination of sliding interfacial shear stress in ceramic matrix composites as long as the debond stress is low (compared with the peak applied stress) and the magnitude of sliding is sufficiently large compared with the displacement resolution of the instrument. In the present study, values of interfacial shear stress below 50 MPa could be readily measured.

2. The lowest value of interfacial shear stress was obtained for carbon-coated fibers in the ALBO fabricated using the polymeric binder. However, this coating was not stable during heat treatment at 1200°C.

3. The application of post-heat treatments to the ALBO fabricated using the polymeric binder was generally detrimental to the sliding characteristics. However, a modest lowering of interfacial shear stress was obtained for the heat-treated ALBO samples processed with aqueous binders containing fibers with the duplex coating.

4. The relative values of modulus and hardness in the fiber-matrix interphase of composites could be quantitatively determined using the MPM.

Acknowledgements

We would like to thank Ms. R. Jackson and Dr. J. V. Cathcart of the Mechanical Properties User Center in the High Temperature Materials Laboratory, Oak Ridge National Laboratory, for the kind assistance during the course of this work. The CMC samples provided by Drs. S. P. Ray and R. A. Marra and the CMC Staff of Alcoa Technical Center are appreciated. The metallographic samples prepared by Mr. J. C. Vilsack of Alcoa Technical Center are also acknowledged.

This research was sponsored in part by the U.S. Department of Energy, Assistant Secretary for Conservation and Renewable Energy, Office of Transportation Systems, as part of the High Temperature Materials Laboratory Program, under contract DE-AC05-84OR21400 with Martin Marietta Energy Systems, Inc.

References

1. P. J. Lamicq *et al.*, "SiC/SiC Composite Ceramics," *Amer. Ceram. Soc. Bull.* **65**(2), 336–338 (1986).
2. K. M. Prewo and J. J. Brennan, "High-Strength Silicon Carbide; Fiber-Reinforced Glass-Matrix," *J. Mater. Sci.* **15**, 463–468 (1980).
3. D. B. Marshall and A. G. Evans, "Failure Mechanism in Ceramic-Fiber/Ceramic-Matrix Composites," *J. Amer. Ceram. Soc.* **68**(5), 225–231 (1985).
4. B. Budiansky, J. W. Hutchinson and A. G. Evans, "Matrix Fracture in Fiber-Reinforced Ceramics," *J. Mech. Phys. Solids* **34**(2), 167–189 (1986).
5. D. C. Phillips, "Interfacial Bonding and the Toughness of Carbon Fiber Reinforced Glass and Glass-Ceramics," *J. Mater. Sci.* **9**, 1847–1854 (1974).
6. L. J. Broutman, in *Interfaces in Composites, **ASTM STP 452*** (American Society for Testing and Materials, Philadellphia, 1969), p. 27.
7. P. S. Chua and M. R. Piggott, "The Glass Fibre-Polymer Interface: I-Theoretical Consideration for Single Fibre Pull-out Tests, *"Composites Sci. and Technol.* **22**, 33–42 (1985).
8. B. Miller, P. Muri, and L. Rebenfeld, "A Microbond Method for Determination of the Shear Strength of a Fiber Resin Interface," *Composites Sci. and Technol.* **28**, 17–32 (1987).
9. H. F. Wu and C. M. Claypool, "An Analytical Approach of the Microbond Test Method Used in Characterizing Fiber/Matrix Interface," *J. Mater. Sci. Lett.* **10**, 260–262 (1991).
10. H. F. Wu and C. M. Claypool, "A Finite Element model of the Use of the Microbond Test Method for Characterization of Composite Interfacial Properties," *J. Mater. Sci. Lett.* **10**, 1072–1075 (1991).
11. L. T. Drzal, M. J. Rich, and P. F. Lloyd, "Adhesion of Graphite Fibers to Epoxy Matrics: I. The Role of Fiber Surface Treatment," *J. Adhesion* **16**, 1–30 (1982).
12. W. A. Frazer, F. H. Ancker, A. T. DiBenedetto, and B. Elbirli, "Evaluation of Surface Treatments for Fibers in Composite Materials," *Polym. Composites* **4**, 238–248 (1983).
13. A. N. Netravali, Z. -F. Li, W. H. Sachse, and H. F. Wu, "Determination of Fiber/Matrix Interfacial Shear Strength by an Acoustic Emission Technique," *J. Mater. Sci.* **26**, 6631–6638 (1991).
14. H. F. Wu, G. Biresaw, and J. T. Laemmle, "Effect of Surfactant Treatments on Interfacial Adhesion in Single Graphite/Epoxy Composites," *Polym. Composites* **12**, 281–288 (1991).
15. J. F. Mandrel, D. H. Grande, T. H. Tsiang, and F. J. McCarry, "A Modified Microdebonding Test for Direct *in-situ* Fiber/Matrix Bond Strength Determination in Fiber Composites," ***ASTM STP 893*** (American Society for Testing and Materials, Philadelphia, 1986), p. 87.
16. D. B. Marshall and W. C. Oliver, "Measurement of Interfacial Mechanical Properties in Fiber Reinforced Ceramic Composites," *J. Amer. Ceram. Soc.* **70**, 542–548 (1987).
17. D. B. Marshall and W. C. Oliver, "An Indentation Method for Measuring Residual Stresses in Fiber Reinforced Ceramics," *Mater. Sci. and Eng.* **A126**, 95–103 (1990).
18. H. F. Wu and M. K. Ferber, "Interfacial Mechanical Properties Characterization of Nicalon SiC Fiber/Alumina-based Composites," Alcoa Research Report No. 57–92–08, Alcoa Technical Center, Alcoa Center, PA (1992).
19. M. F. Doerner and W. D. Nix, *J. Mater. Res.* **1** [4], 601–9 (1986).